ADVANCED MATERIALS INTERFACES
Open Access
www.advmatinterfaces.de

Adsorption, Single-Molecule Manipulation, and Self-Assembly of Borazine on Ag(111)

*Tobias Weiss, Aleksandr Baklanov, Georg S. Michelitsch, Karsten Reuter, Martin Schwarz, Manuela Garnica, and Willi Auwärter**

The interaction of borazine with metal supports and the concomitant surface chemistry play important roles in the synthesis of hexagonal boron nitride and the assembly of BN-doped carbon nanostructures, thus making adsorbed borazine an intriguing model system. Herein, the first real space characterization of individual borazine molecules and highly ordered borazine self-assemblies on solid supports, combining scanning tunneling microscopy (STM), scanning tunneling spectroscopy, X-ray photoelectron spectroscopy, and complementary density functional theory modeling is reported. Specifically, a weak, nondissociative adsorption of borazine with the ring aligned in parallel to the surface plane is observed on Ag(111) upon low temperature deposition. Borazine is found to favor hollow adsorption sites, which guide the assembly of intricate borazine assemblies including a porous, chiral honeycomb-like network, and dense-packed monolayer films. Additionally, a modification of the borazine adsorption configuration by STM-based manipulation is demonstrated. Dehydrogenation of individual molecules by voltages pulses yields an upright standing borazine fragment bound via B to Ag. This study thus provides a comprehensive, single-molecule level characterization of borazine adsorption and surface chemistry on a characteristic coinage metal support and may serve as a reference for advanced low-dimensional materials based on functionalized borazines or including BN units as dopants.

1. Introduction

Borazine, $(HBNH)_3$, the isostructural and isoelectronic analogue to benzene, keeps attracting considerable interest in modern science, even nearly a century after its first synthesis, reported in 1926 by Stock and Pohland.[1] Fundamental conceptual issues, such as aromaticity in borazine and its relation to benzene, are still debated, pointing to its relevance as model system.[2,3] Furthermore, borazine is heavily employed in material science applications,[4] including low-dimensional materials,[5,6] ceramics,[7] and optoelectronic devices.[8,9] However, only few studies address pristine borazine adsorption on metal surfaces under ultrahigh-vacuum (UHV) conditions well below room temperature. Specifically, borazine adsorption was experimentally studied on Re(0001),[10] Ru(0001),[11] Rh(111),[12,13] Ir(111),[14] Pt(111),[15,16] *h*BN/Pt(111),[15] Pt(110),[17] and Au(111)[16] with space-averaging surface science methods, revealing intricate behavior. Borazine might adsorb flat, i.e., with the $(BN)_3$ ring aligned in parallel with the surface plane, or upright, even in the (sub)monolayer regime. Thereby, nondissociative adsorption can compete with dissociative adsorption, where the latter might feature B- or N-terminal dehydrogenated borazine. For example, on Pt(110), a borazine monolayer adsorbed at 110 K includes intact, flat lying borazine as well as upright borazine species that underwent H abstraction.[17]

Additionally, the adsorption of pristine borazine on metal surfaces gained considerable attention in the last decades due to eminent role of borazine as precursor for chemical vapor deposition (CVD) growth of hexagonal boron nitride (*h*BN) monolayers.[5,18] *h*BN is an important representative of the 2D materials library, where reliable synthesis protocols are indispensable in order to achieve high quality and durability.[5,19–22] In this context, borazine is usually dosed at high temperatures (> 800 K) on catalytically active metal supports,[18] thus complementing the low temperature adsorption studies addressed above. In particular, the UHV-based CVD synthesis route to *h*BN can involve different adsorption configurations of the borazine precursor (i.e., orientations of the borazine ring relative to the metal surface

T. Weiss, A. Baklanov, M. Schwarz, M. Garnica, W. Auwärter
Physics Department E20
Technical University of Munich
85748 Garching, Germany
E-mail: wau@tum.de
G. S. Michelitsch, K. Reuter
Fritz-Haber-Institut der Max-Planck-Gesellschaft
14195 Berlin-Dahlem, Germany
M. Garnica
Instituto Madrileño de Estudios Avanzados en Nanociencia (IMDEA-Nanociencia)
Madrid 28049, Spain

The ORCID identification number(s) for the author(s) of this article can be found under https://doi.org/10.1002/admi.202300774

DOI: 10.1002/admi.202300774

plane), as well as dehydrogenation and dissociation.[12,14,17,23] Whereas dissociation of the $(BN)_3$ ring is reported for *h*BN growth on Re(0001), Ir(111), and Rh(111),[13] dendritic *h*BN morphologies on Cu(111) were attributed to intact $(BN)_3$ rings during growth.[24] As recently reported for Ru(0001), intermediate porous phases constituted by dehydrogenated borazine might exist during *h*BN synthesis.[25]

Furthermore, considerable organic synthesis efforts gave access to a variety of borazine derivatives,[4,26] covering structures ranging from halogenated borazines[27] to complex functionalized borazines.[28–30] These serve as versatile building blocks, integrating the $(BN)_3$ ring into carbon scaffolds.[31] On solid supports, self-assembly protocols and on-surface reaction schemes have been applied to functionalized borazines, yielding patterned surfaces exposing polar BN bonds[31–34] and BN-doped covalent carbon nanostructures on metal supports.[35]

Considering all the aspects introduced above, the adsorption configuration and self-assembly of unsubstituted borazine on coinage metal supports, as well as its multi-faceted chemistry yielding to borazine decomposition, is of general interest. On the one hand, borazine with its C_3 symmetry and minimal size is a promising building block, anticipated to form self-assembled honeycomb-like structures with regular pores.[36,37] On the other hand, individual borazine molecules represent a model system to investigate adsorption characteristics and single-molecule chemistry. Surprisingly, we are not aware of any study reporting real-space imaging of borazine and its supramolecular assemblies on solid supports, or addressing reactions such as borazine dehydrogenation on the single molecule level.

Here, we provide the first real-space imaging of surface-supported pristine borazine molecules. Specifically, we report on distinct self-assembled borazine structures on Ag(111) and demonstrate controlled dehydrogenation of single borazine molecules. A detailed characterization of individual molecules and two distinct self-assembled phases, namely a porous phase and a dense-packed phase, is accomplished via low temperature STM measurements. The different assemblies are achieved by adjusting the borazine dosage and each of the structures exhibit domains of organizational chirality formed by intact and flat lying borazine molecules. Insights about the interaction with the substrate are obtained through scanning tunneling spectroscopy (STS). Furthermore, the adsorption geometry is modified by manipulation of individual borazine molecules via tip-induced voltage pulses, promoting dehydrogenation. This reaction yields an upright standing configuration of the molecule. Density functional theory (DFT) calculations are employed to explore the adsorption energies and sites of the intact borazine molecules on the Ag(111) support and to identify a main manipulation product as dehydrogenated borazine species bound via B to Ag.

2. Results

2.1. Self-Assembly and Adsorption Configuration

Figure 1a–d presents STM data upon adsorption of a small amount of borazine (dose ≈0.01 L) on the Ag(111) substrate at 150 K. The overview image in Figure 1a shows extended molecular islands featuring regular arrays of pores with a periodicity of (25.4 ± 0.5) Å. The pores constitute a hexagonal lattice and the image reveals coexisting domains with distinct orientations. A more detailed examination (see intermediate scale image in Figure 1b) indeed shows two distinct domains and resolves each borazine molecule as individual protrusion. The red and blue rhombi in Figure 1b highlight the respective unit cells of the two domains and enclose an angle of (32 ± 4)°. The unit cells are rotated by ± (16 ± 4)° with respect to the [1–10] and equivalent Ag(111) crystal directions. Figure 1c shows the image obtained by the fast Fourier transformation (FFT) routine applied to the STM image in Figure 1b. It emphasizes the two hexagonal patterns, where the spots originating from each of the domains are encircled in red and blue, respectively. Reflecting the STM images, the two sublattices are rotated by 32° toward each other. Interestingly, few pores inside the regular porous structure are filled with an additional molecule (see Figure 1b, marked with black arrow). The high-resolution image shown in Figure 1d reveals additional insights into the molecular packing scheme. Each unit cell includes twelve molecules that are arranged into two triangular subunits of six molecules, as highlighted by the black triangles in Figure 1d. Particularly, any two neighboring triangular subunits are arranged with a small lateral offset along their common side of the triangles. The direction of this shift is specific to each of the domains and thus expresses the chirality of the system. Note that the [1–10] and equivalent Ag(111) directions are identified as mirror axes for these chiral domains. Moreover, the characteristic hexagonal assembly arises from grouping six triangular subunits around a central pore. This architecture features three molecules along the side of each triangular subunit and is thus classified as N = 3 porous honeycomb-like structure following the notation for C_3-symmetric molecules in ref. [37].

After dosing larger amounts of borazine (≈0.18 L) onto the substrate held at 150 K, an additional dense-packed phase is observed (see overview image in Figure 1e). In contrast to the low exposure case, this dense-packed phase is characterized by striped patterns. This assembly differs from the porous structure, even if all its central pores were filled by additional borazine molecules. Domains with distinct orientations of the stripes coexist, as can be seen on the adjacent terraces in Figure 1e. High-resolution imaging (Figure 1f) reveals a grouping of molecules into pairs (with dumbbell-like appearance), highlighted by white ellipses. The different alignment of the pairs gives rise to the striped pattern, which includes rows with a width of two or three borazine molecules. Alternating pairs lead to the two-striped pattern (marked by green arrows). Stacking two pairs with the same orientation and one pair of the alternative orientation results in the three-striped configuration (yellow arrows).

After this rather general description of the porous network and the dense-packed striped borazine assembly, we now proceed to a more detailed characterization of these borazine architectures and their interaction with the supporting Ag(111) lattice, also discussing individual borazine molecules. To this end, **Figure 2** presents additional STM data and complementary DFT-based STM image simulations. The overview image including a border of a porous assembly and adjacent individual species (Figure 2a) resolves distinct borazine molecules and their orientation. As emphasized in Figure 2b, individual borazine molecules appear as triangular-shaped protrusions with a depression at each side of the triangles, allowing identifying the orientation of the molecules. Judging from the STM data, the borazine

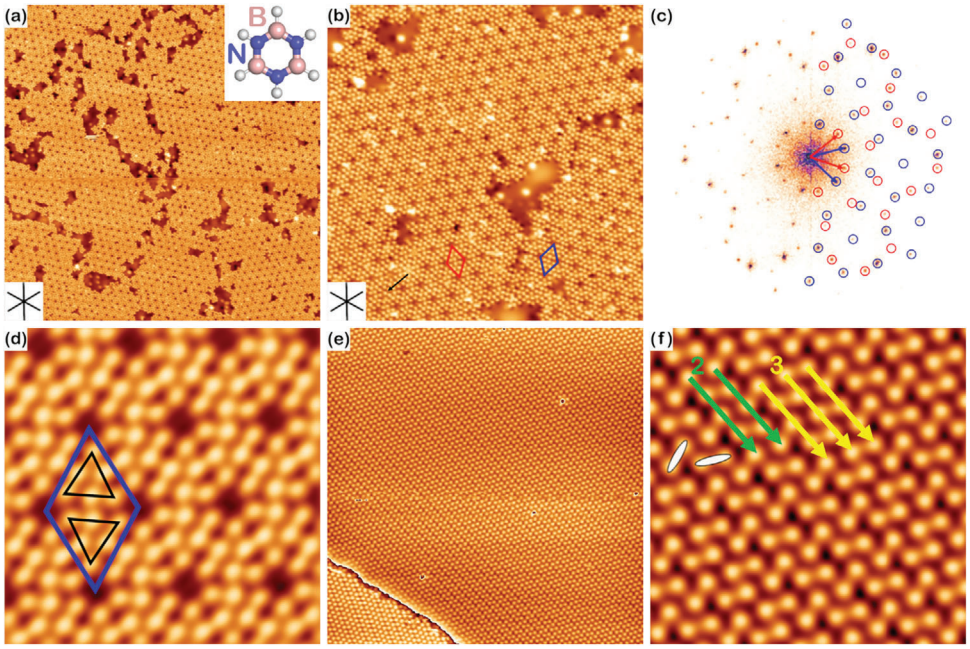

Figure 1. Characteristic structures formed by borazine molecules on Ag(111): a–d) Porous honeycomb-like assembly and e,f) dense-packed assembly. a) Overview STM image of the low exposure phase. An enlarged image is provided in Figure S1a (Supporting Information). The molecular structure of borazine is shown in the top right corner. b) Intermediate scale image showing two chiral domains each consisting of a hexagonal arrangement, where the respective unit cells are highlighted with red and blue frames. c) Corresponding FFT image featuring a superposition of two hexagonal patterns each originating from one of the chiral domains. Blue and red circles, superimposed on the right half of the image, indicate the spots attributed to the marked domains in (b). The unit cell vectors in reciprocal space are k = 0.45 nm^{-1} long . d) High-resolution STM image. The blue rhombus highlights the unit cell and each triangle (marked in black) shows the arrangement of six molecules. e) STM image of the dense-packed phase featuring a striped pattern, which exhibits distinct orientations on adjacent terraces (contrast adapted for visibility, for raw data, see Figure S1, Supporting Information). f) Zoomed-in image unveiling the striped pattern, which comprises of rows of two (green arrows) and three (yellow arrows) molecules, respectively. The white ellipses mark shorter intermolecular distances. The black cross in the inset of (a,b) mark the [1-10] and equivalent Ag(111) directions. [Imaging parameters: a) 107.5 × 107.5 nm^2, 0.05 V, 0.5 nA b) 43.7 × 43.7 nm^2, −0.05 V, 0.5 nA d) 8.6 × 8.6 nm^2, −0.1 V, 0.5 nA e) 36.6 × 36.6 nm^2, 0.05 V, 0.5 nA f) 8.6 × 8.6 nm^2, 0.25 V, 1 nA].

molecules adsorb "flat" on Ag(111) (i.e., with the borazine ring aligned parallel to the Ag surface plane), show a threefold symmetry (C_3, reflecting the molecular structure), and occur in two distinct orientations, rotated to each other by 180° (see Figure 2b). To rationalize these observations, we performed STM image simulations based on DFT-optimized interface structures of borazine on a Ag(111) slab. These STM simulations (Figure 2c) reveal a triangular shape of individual borazine molecules, where the corners and sides of the triangle are attributed to the positions of boron (represented in pink in the model) and nitrogen (blue in the model). The agreement of the molecular appearance, showing a triangular outline, between the simulated and experimental STM images , indicates a nondissociative adsorption of borazine molecules on Ag(111) (Figure 2b,c, see Discussion section). Characterization by complementary X-ray photoelectron spectroscopy (XPS), shows different binding energies compared to hexagonal boron nitride on Ag(111)[38] and does not indicate (partial) borazine dissociation or decomposition (Figure S2, Supporting Information). The calculated triangular shape persists for different packing densities (Figure S3, Supporting Information) and for fcc and hcp adsorption sites (Figure 2c). However, these two distinct adsorption sites yield two configurations that differ by rotation of (integer multiples of) 60° around the C_3-symmetry axis of the molecule. In both cases the B–B and N–N axes are aligned with the [1–10] and equivalent Ag(111) directions. Accordingly, we assigned the two distinct borazine orientations observed experimentally to fcc and hcp adsorption sites. Calculations for the alternative adsorption sites (Figure S4, Supporting Information) yield orientations not compatible to the experimental observations. To highlight the molecular orientation, a pink-colored triangle (with its corners near the boron atoms) is superimposed jointly with a structural model on the STM data of a borazine molecule in Figure 2b.

Next, the azimuthal orientation of the borazine molecules in the porous phase is deduced from their triangular-shaped appearance and the depressions at the borders of an island (compare Figure 2a). The characteristic alignment of the borazine molecules with the [1–10] and equivalent directions observed for individual molecules is maintained in this assembly. The twelve molecules in the unit cell (blue rhombus, compare Figure 1b,c) feature two distinct orientations (Figure 2e), marked by blue and pink triangles. As mentioned above, chiral domains in this porous phase originate from the chiral assembly in the unit cell, featuring a lateral shift of the two triangular unit cell halves. Interestingly, a specific arrangement of borazine molecules is observed within each half of the unit cell. Three molecules of the same orientation are grouped into a triangle and are surrounded by three molecules of the opposite orientation located at the

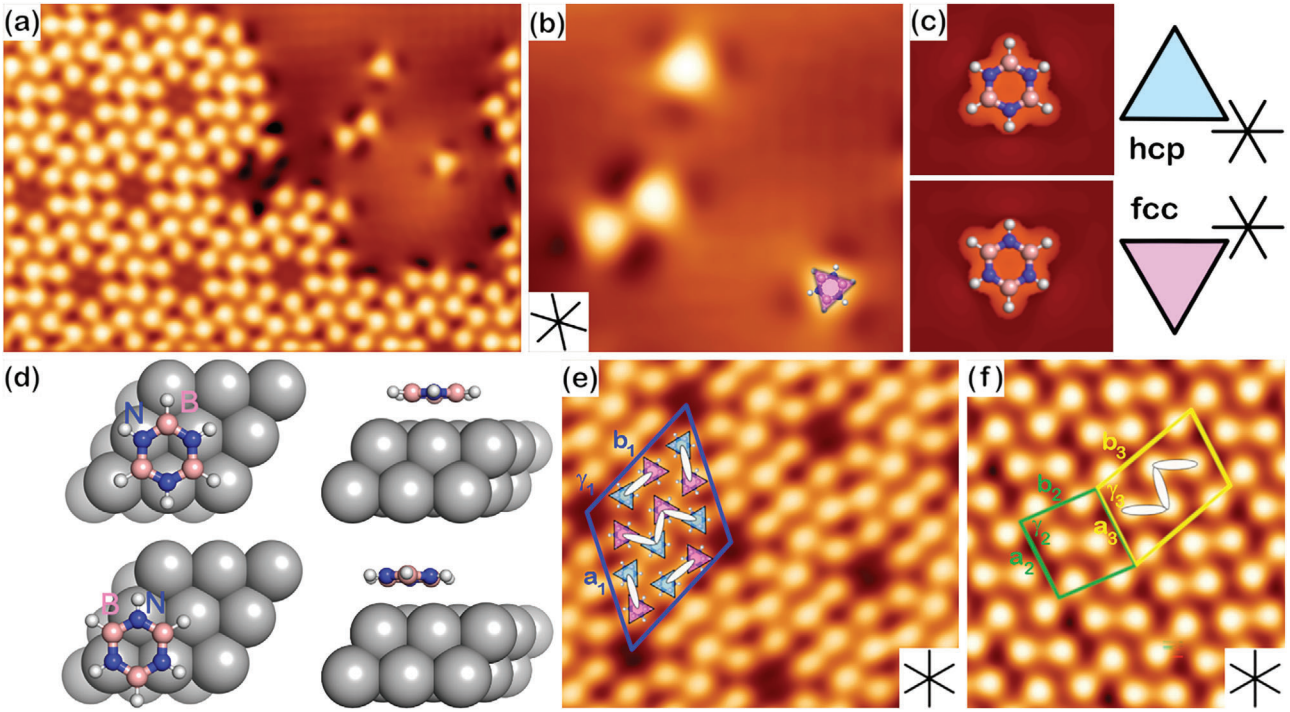

Figure 2. a) High-resolution STM image of individual borazines near a border of a porous assembly on Ag(111). b) Individual molecules appear as triangular protrusions surrounded by three depressions. A molecular model (B: red, N: blue) is superimposed. c) Simulated STM images of borazine molecules adsorbed on fcc and hcp sites of a Ag(111) slab. d) Corresponding DFT-optimized structural models for the hcp (top panel) and fcc sites (bottom panel) with top and side views, respectively. e) The unit cell of the porous phase comprises 12 molecules, gathered into two triangular subunits of six molecules each. The two orientations of borazine are color-coded (blue and pink, respectively), shorter intermolecular distances are highlighted in white. f) The unit cells of the two- and three- stripe patterns are marked by green and yellow frames. Both unit cells involve pairs of molecules with two distinct orientations that are located at their corners and centers. The three-stripe pattern features two parallel pairs in the center of the unit cell, while the two-stripe pattern hosts only one pair. The black crosses in the insets mark the [1-10] and equivalent Ag(111) directions. [Imaging parameters: a) 12.7 × 8.6 nm^2, −0.1 V, 0.5 nA b) 4.0 × 3.8 nm^2, −0.1 V, 0.5 nA c) Simulation: −0.1 V e) 6.9 × 6.0 nm^2, −0.1 V, 0.5 nA f) 4.9 × 5.4 nm^2, 0.25 V, 1 nA].

corners of the triangular half unit cell. The borazine orientations are reversed for the respective other half of the unit cell. Moreover, adjacent molecules of different orientations are grouped into pairs by shorter intermolecular distance of (6.4 ± 0.5) Å, as highlighted by white ellipses in Figure 2e, compared to the distance to the other molecules that is measured as (7.3 ± 0.5) Å. These pairs represent the building blocks of the assemblies. The lateral offset between the two molecules induces a chiral nature of the pair, which translates to the chirality of the assembly, introduced above. Potential driving forces for the pair formation are addressed in the discussion section. The unit cell of the porous phase has dimensions of $a_1 = b_1 = (25.4 \pm 0.5)$ Å and encloses an angle of $\gamma_1 = (119 \pm 3)°$.Compare also Figure S11 (Supporting Information) for a tentative structural model of the assembly and matrix notation.[39]

For the dense-packed phase, high-resolution imaging (Figure 2f) reveals discernible repeating units (which we refer to as unit cells) of the two- and three-stripe patterns as illustrated in Figure 2f with green and yellow frames, respectively. The dimensions of the two-stripe unit cell are $a_2 = (13.6 \pm 0.3)$ Å and $b_2 = (12.3 \pm 0.4)$ Å with an enclosed angle of $\gamma_2 = (87 \pm 4)°$. Whereas the three-stripe unit cell is spanned by $a_3 = (13.1 \pm 0.2)$ Å and $b_3 = (18.4 \pm 0.5)$ Å with an angle $\gamma_3 = (102 \pm 4)°$. Similar to the low exposure case, the molecules show distinct orientations relative to the [1–10] and equivalent Ag(111) directions in this phase (Figure S5, Supporting Information). Additionally, in both stripe patterns the molecules are arranged in pairs by their intermolecular distance, as highlighted by white ellipses in Figure 2f. In particular, the short distances for the two- and three- stripe patterns are (6.1 ± 0.5) Å and (5.7 ± 0.5) Å, respectively. The long distances amount to (7.1 ± 0.5) Å and (7.0 ± 0.5) Å.

The packing densities ρ of the three assemblies are $\rho_{\text{porous}} = (2.1 \pm 0.1)$ molecules nm^{-2}, $\rho_{\text{two-stripe}} = (2.4 \pm 0.1)$ molecules nm^{-2}, and $\rho_{\text{three-stripe}} = (2.5 \pm 0.1)$ molecules nm^{-2}, showing that the striped patterns are denser than the porous structure, in accordance with the preparation.

The STM data clearly signal an influence of the Ag(111) support on the borazine orientation and position. To understand the interaction of borazine with the substrate, the adsorption energetics of the molecules are addressed by DFT calculations. The analysis of adsorption height and energy for different adsorption sites (Table S1, Supporting Information) reveals that the adsorption energy for borazine molecules on high-symmetry sites is ≈0.8 eV at an average distance of 3.3 Å from the metal facet, indicating physisorption. Considering the alignment of the borazine molecules with the [1–10] and equivalent Ag(111) directions in the porous phase, we identify the fcc and hcp sites as the energetically most favorable positions compared to the on-top and bridge sites.

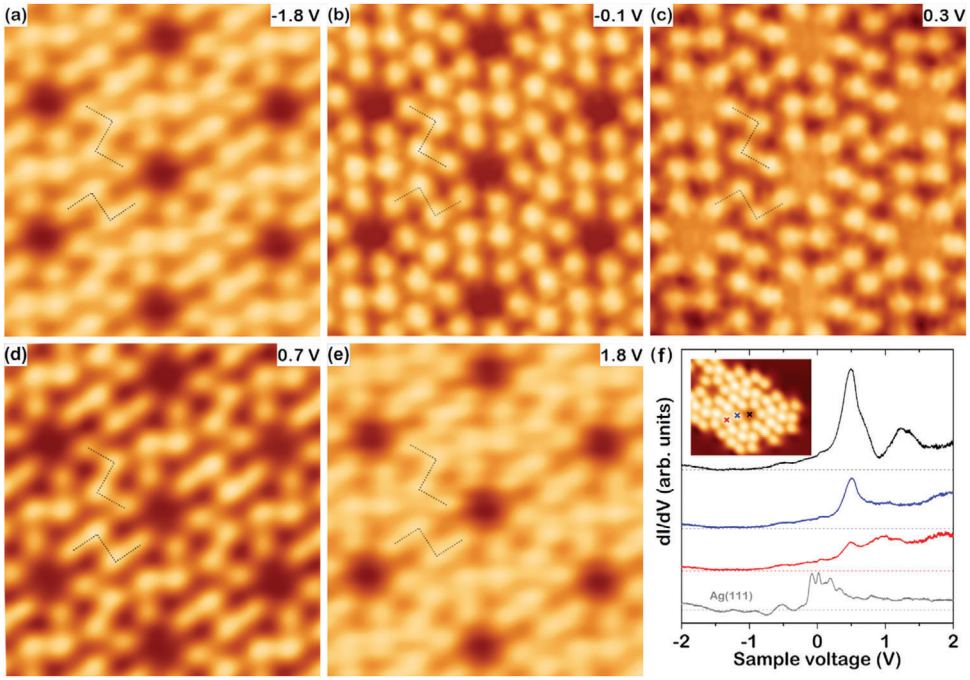

Figure 3. Interfacial electronic structure of the porous borazine phase. a–e) Bias dependent STM images. At negative sample bias voltage each molecule appears as a single lobe. Around 0.3 V, the pores appear "filled" (c), which correlates with the main peak in the corresponding spectrum (f). Around 0.7 V, the lobes appear connected, leading to a "z"-shape contrast comprised of four molecules (d) that persists at higher voltage (e). f) Scanning tunneling spectra recorded at the pore and above two selected positions of molecules in the assembly are marked with black, red, and blue crosses respectively. A reference spectrum on bare Ag(111) is provided for comparison. The spectra are vertically offset for better visibility, dashed lines mark the respective zero offset. [Imaging parameters: a) 5.7 × 6.0 nm^2, 0.3 nA b) 5.7 × 6.0 nm^2, 0.3 nA c) 5.7 × 6.0 nm^2, 0.2 nA d) 5.7 × 6.0 nm^2, 0.3 nA (e) 5.7 × 6.0 nm^2, 0.3 nA f) 7.6 × 6.0 nm^2 −2.0 V, 0.21 nA].

However, the differences observed in the adsorption energies are very small, with the largest deviation being 0.06 eV (see Discussion section). Accordingly, the occupation of additional adsorption sites (beyond fcc and hcp) cannot be excluded for the dense-packed phase (see Figure S5, Supporting Information).

2.2. Electronic Interface Structure

To probe the interfacial electronic structure of borazine on Ag(111), STS measurements and bias-dependent imaging were performed (**Figure 3**; Figure S6, Supporting Information). A series of STM images of the porous phase recorded at bias voltages between −1.8 and +1.8 V reveals that the appearance of molecules and the contrast of the pores in the assembly are bias-dependent (Figure 3a–e). At negative sample bias voltages, the pores are imaged as depressions and all molecules appear as single protrusions, which is emphasized at low negative voltages (Figure 3b). At positive sample bias voltage around 0.3 V, the pores appear with a brighter contrast (Figure 3c). Around 0.7 V prominent "connections" occur between distinct molecules (Figure 3d), resulting in a characteristic "z"-like appearance, involving four molecules. The apparent "merging" of these four molecules is correlated with three pairs of molecules with shorter intermolecular distances. To further address the electronic structure at different parts of the porous assembly, *dI/dV* spectra are taken above the pores and the center of two selected molecules that exhibit different orientations. The corresponding spectra are shown in black, blue, and red in Figure 3f, respectively. At negative bias voltages, all three spectra appear featureless, while at positive voltages the spectra reveal electronic resonances at 0.5 V. This characteristic peak is most pronounced in the spectrum measured above the pore and is attributed to confinement of the Ag-derived surface/interface state,[40,41] thus explaining the bright appearance of the pores in the STM images at 0.3 V (Figure 3c). The spectrum acquired above the borazine molecule close to the center of the unit cell (red curve) shows a broad feature in the unoccupied states region with its maximum at 0.98 V. Whereas, for the molecules closer to the pore (blue in Figure 3f) the signal intensity at this energy is decreased. This is also reflected in the molecular appearance in STM images at 0.7 V (Figure 3d), where the molecules closer to the pore feature a lower apparent height than the central ones. Overall, the strongest signature in the STS data is attributed to confinement of the Ag-derived electronic surface/interface state in the pores of the assembly. Borazine electronic states might contribute at ≈1 V and ≈2 V.

2.3. Modification of the Adsorption Configuration by Single Molecule Manipulation

So far, we demonstrated the "flat" adsorption configuration of pristine borazine on Ag(111), both in assemblies and for

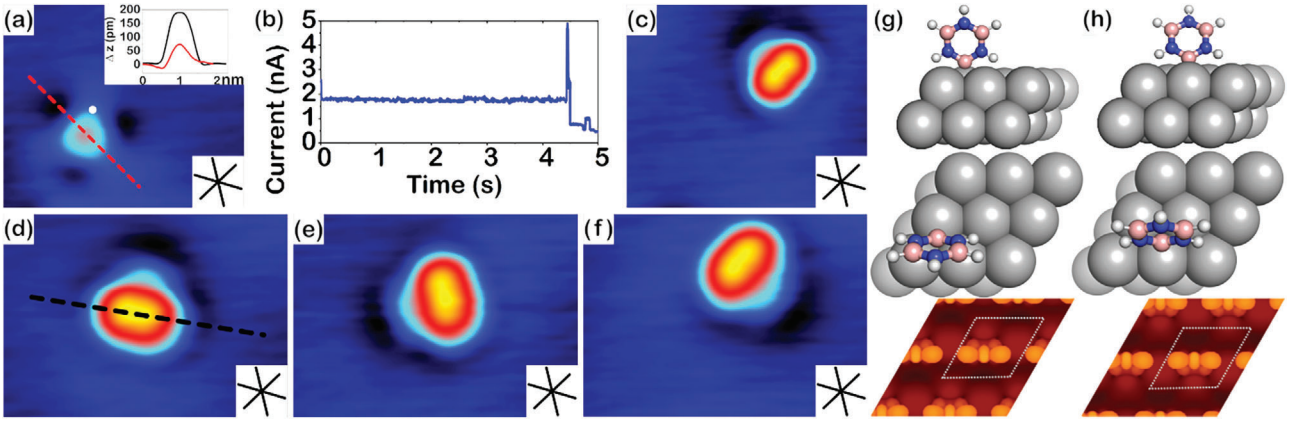

Figure 4. Manipulation of single borazine molecules. The voltage pulse of 2.5 V applied to an isolated borazine molecule at the position marked with a white dot (a) causes a drastic change in the molecular appearance (c). The corresponding current–time sequence recorded during this process reveals several intermediate steps (b). The resulting manipulation product exhibits an elongated shape oriented along one of the [1-10] and equivalent Ag(111) directions. The apparent height changes from 0.7 to 1.9 Å, shown by the line profiles in inset (a). Subsequent voltage pulses result in translation and rotation of the manipulation product (d–f), maintaining the alignment with the crystal high symmetry directions. The STM images (a,c) and (d–f) show the same region of the surface respectively, illustrating the translational part of the movement. DFT simulations of a tilted, B-terminal dehydrogenated borazine molecule adsorbed on fcc (g, top) or hcp (h, top) sites, and the corresponding calculated STM signatures at −0.1 V (g,h, bottom) match the experimental observations of the manipulation product. The dashed rhombi represent the sections of the top panels. Black crosses in the insets mark the [1-10] and equivalent Ag(111) directions. [Imaging parameters: a,c) 2.9 × 2.5 nm^2, −0.1 V, 0.5 nA, z-scale 0.0-1.9 Å (d–f) 2.7 × 1.9 nm^2, −0.1 V, 0.5 nA, z-scale 0.0–1.9 Å]

individual molecules. Considering the different adsorption behavior reported on other substrates (see Introduction section), we venture to demonstrate that even on Ag(111), tilted adsorption configurations can be achieved. To this end, we focus on individual borazine units as a model system. Application of voltage pulses to individual molecules reproducibly results in distinct modifications in contrast, symmetry, and apparent height of the molecules (**Figure 4**; Figure S7, Supporting Information). These changes can be accompanied by translational and rotational movements. Figure 4 summarizes the manipulation sequence and the properties of one characteristic product. The STM images in Figure 4a,c show the very same area of the Ag(111) surface including one borazine molecule, before and after applying a voltage pulse (2.5 V, 5 s) near a boron position of the molecule (position marked in Figure 4a). The current–time trace (Figure 4b) recorded during the voltage pulse shows discrete steps, pointing to several sequential processes during the manipulation (such as chemical modification and displacements). Upon manipulation, the borazine molecule changed its appearance from the characteristic threefold symmetric contrast (discussed above) to an elongated shape featuring a bulge on one side. Additionally, the apparent height is increased from 0.7 to 1.9 Å (see inset in Figure 4a) and the molecule is displaced laterally. The long axis of this bulge-shaped manipulation product is aligned with one of the [1–10] and equivalent Ag(111) directions. This preferred alignment is visualized in the image sequence shown in Figure 4d–f, displaying rotation and further translation of this manipulation product. First, a voltage pulse leads to rotation (d → e). A subsequent pulse then results in a combined rotation and translation (e → f). After each step the product retains its characteristic appearance and its alignment with the primary crystal directions. Such movements can be triggered by voltage pulses up to 3 nm away from the affected molecule, indicating a remote effect on the dynamics of the manipulation product either by the electric field between tip and sample or by hot electrons. No modifications were observed for bias voltages below 2.5 V, consistent with nonperturbative STM imaging at such voltages (see Figure 3).

In order to identify this characteristic manipulation product, DFT simulations were performed for various B- and N-terminal dehydrogenated (Figure 4; Table S2; Figure S8, Supporting Information) and deprotonated borazine fragments (Table S3, Figure S9, Supporting Information) as well as for doubly dehydrogenated borazine species (Table S4, Figure S10, Supporting Information) on distinct adsorption sites of the Ag(111) surface. For the B-terminal, single dehydrogenated species adsorbed on the fcc (Figure 4g) and hcp (Figure 4h) sites, the simulated STM images are in good agreement with the experimental observations. Notably, the alignment with the crystal directions and the elongated, rod-like appearance with a bulge are reproduced. None of the other configurations matches the experimental observations well (Figures S8–S10, Supporting Information); the B-terminal adsorption sites are preferred over the N-termination (Table S2 and S3, Supporting Information). Thus, the manipulation product is assigned to such an upright standing, singly dehydrogenated borazine molecule, exposing a B atom to the Ag support. The increase of the apparent height in STM images upon manipulation is consistent with an upright standing geometry. The calculated adsorption energy at the fcc and hcp sites is nearly identical for this singly dehydrogenated B-terminal species (see Table S2, Supporting Information), pointing to the possible occupation of fcc and hcp sites.

3. Discussion

We first discuss the adsorption behavior of borazine. The STM data complemented by an XPS analysis and STM image simulations indicate that borazine adsorbs intact on Ag(111) at low temperatures, with the plane of the borazine molecule parallel

to the Ag surface (i.e., flat). This is not unexpected, as even on more reactive (111) surfaces, dehydrogenation only starts at elevated temperatures (e.g., ≈300 K for Ni(111)[23]). The "footprint" of one borazine derived from the molecular areal density of the dense-packed assemblies amounts to about 42 Å^2, closely matching values reported for the flat adsorption of intact borazine on Ru(0001) (41.3 Å^2)[11] and clearly exceeds the 18.5 Å^2 deduced for tilted, dehydrogenated borazine on Pt(111).[11] This corroborates a nondissociative, flat adsorption, which thus seems characteristic for rather inert supports (such as Au and *h*BN).[15,16] In contrast to several other metal supports (including Rh(111), Ir(111), Pt(111)), we did not observe a combination of flat and upright adsorption configurations on Ag(111) for intact borazine in the achieved coverage range.

In this study, the self-assembled borazine structures are formed on Ag(111) by adjusting the borazine dose at substrate temperatures below 150 K. After warming up to room temperature, borazine completely desorbed from Ag(111), consistent with the absence of borazine after room temperature exposure. On Pt(111)[16] and Au(111)[16] a multilayer desorption routine in the temperature range 135–150 K was applied to achieve monolayers of borazine. Thus, similar – and low – temperatures are needed to adsorb intact borazine on these different unreactive metal supports.

The STM data demonstrate two distinct azimuthal orientations of intact borazine on the Ag(111) lattice, which are identical for individual borazine species and molecules constituting the porous self-assembled structure. As borazine shows a triangular appearance in high-resolution STM images, these two orientations are represented by triangles pointing in opposite directions. Individual borazines on Ag terraces and molecules at borders of islands exposing a side of triangle to the bare Ag areas show distinct depressions in STM images recorded at low bias voltage. These depressions are tentatively attributed to electron density depletion near the N–H positions, due to the localization of negative charge at the nitrogen atoms, reminiscent of earlier STM findings on molecules featuring terminal N on Ag(111).[42] This STM contrast is thus consistent with the assignment of the N positions of the borazine ring to the sides of the apparent triangle. The STM image simulations do not reproduce the depressions near the molecules, which we attribute to limitation of the modeling approach (e.g., s-wave tip character) in properly describing localized electronic features.

A precise evaluation of the molecular positions and intermolecular distances in the porous honeycomb phase (see Figure 2b; Figure S11, Supporting Information) reveals that borazines occupy two different adsorption sites of the Ag(111) lattice. These two adsorption sites are reflected in the two opposite borazine orientations. A statistical analysis of 138 individual molecules reveals an fcc:hcp ratio of 59:41 between the two orientations, whereas in the islands the orientations of the molecules are equally distributed (50:50). By comparison to the DFT calculations, we assign the two adsorption sites to configurations with the center of the borazine ring on fcc and hcp hollow sites, respectively. Whereas the calculations for other symmetric adsorption sites, such as on-top or bridge, yield similar adsorption energies (compare Table S1, Supporting Information) the alignment of the triangular outline of the borazine with the [1–10] and equivalent Ag(111) directions observed in the STM data matches only the two hollow sites. In both adsorption configurations, the nitrogen atoms (colored blue in the model) are located (roughly) on top of Ag atoms (see Figure 2d). Such a configuration with nitrogen above on top and boron above hollow sites is known as stable configuration for *h*BN on Ni(111)[43] and predicted to be the favorite registry for *h*BN on other transition metals.[44,45] For Ag(111), however, *h*BN is calculated to be repelled even in this configuration[38] and to be only weakly bonding in a rotated 2 × 2 *h*BN unit cell.[45] Experiments indeed do not reveal preferred azimuthal orientations of *h*BN domains.[38] Accordingly, our findings for individual borazines and self-assembled borazine films on Ag(111) reveal an adsorption behavior distinctly different from *h*BN/Ag(111).[38]

The calculated adsorption energies for borazine on Ag(111) confirm a weak adsorption, and do not suggest considerable site-specific interactions between individual borazine molecules and Ag(111). Nonetheless, the STM imaging revealed an important role of the substrate, inducing two distinct adsorption sites/orientations, yielding the intricate honeycomb network. Also, the assembly into striped arrays reveals distinct molecular orientations. A common feature of these assemblies is the grouping of molecules into apparent pairs with short intermolecular distance, which originate in the two coexisting adsorption configurations. In the porous case, two adjacent pairs appear as z-shape, while for the dense-packed cases, the pairs appear as separated dimers or z-shaped structures (see Figure 2e,f). Computational modeling of isolated borazine dimers was reported to yield several minima in the potential energy landscape, including a configuration with laterally displaced borazines in an antiparallel alignment and a center-to-center distances of 6.5 Å (not representing the global minimum in gas phase, though).[46,47] Electrostatic interactions emerging from the polar BN bonds might contribute to stabilize the on surface-assemblies. Interestingly, the transition from the porous assembly to the dense-packed phases follows a different scheme than previously reported for other C_3-symmetric molecules,[37] where honeycomb assemblies with an increasing number (N) of molecules along the side of the triangular subunits were formed upon increasing the coverage. Here, only a single honeycomb-like pattern (with N = 3) is observed for all borazine exposures resulting in the porous phase. The arrangement of the molecules in two chiral domains in the porous phase resembles indeed reported chiral assemblies of other C_3-symmetric molecules.[36,48,49] The lateral shift between the triangular subunits can be used to categorize the assemblies. A shift of a complete triangle would result in a Kagome-lattice, while no shift would yield a perfect honeycomb lattice. The present porous borazine assembly is thus recognized as an intermediate structure between a Kagome and honeycomb lattice, labeled honeycomb-like.

The porous borazine assembly leads to surface state confinement effects in the pore areas exposing bare Ag, thus tailoring the surface electronic landscape.[40] The electronic signature of the pores persists in spectra recorded above adjacent borazines, indicating a weak interaction of the pristine molecule with the metal. Contributions from an electronic interface state in borazine-covered areas are not evident in our STS data. In contrast, an interface state was observed for borazine derivatives on Cu(111) and Ag(111), which were functionalized to reduce molecule – substrate interactions and to promote network formation.[32] An

interface state slightly upshifted from the pristine Ag(111) surface state was also reported for *h*BN/Ag(111).[50] The apparent absence of borazine-derived electronic states near the Fermi level and down to binding energies of at least 2 eV (i.e., −2 V sample voltage, see Figure 3f) is consistent with photoemission results of borazine on Pt(110).[17]

We now proceed to address the characteristic product achieved by STM manipulation of individual borazines, briefly expanding on the results obtained by DFT. Spin-polarized calculations were performed for a neutral borazine-fragment and an anionic borazine-fragment adsorbed on different positions of a 3 × 3 × 3 Ag(111) supercell. Different adsorption sites (on top, fcc, hcp, bridge) in a B-terminal or N-terminal configuration were screened for a dehydrogenated/deprotonated reaction product (Figures S8–S10, Supporting Information). In agreement with previously reported studies of a dehydrogenated borazine reaction product on Pt, the B-terminal adsorption site is preferred over N-terminal.[17] No stable adsorption position in the N-terminal studies apart from on-top was obtained. In conjunction with the experimental evidence for alignment along the [1–10] and equivalent Ag(111) directions and the asymmetric appearance in STM imaging (rod-like shape with a bulge on one side), the manipulation product is identified as a singly dehydrogenated B-terminal borazine. It adsorbs upright with a minor tilt and might occupy fcc and hcp sites (see Figure 4g,h). Other adsorption configurations including deprotonated and ortho- and para-doubly dehydrogenated borazine molecules on various adsorption sites do not provide a better match with the experimental findings (see Figures S8–S10, Tables S2–S4, Supporting Information). While this singly dehydrogenated upstanding borazine fragment was achieved reproducibly from pristine borazine and could be rotated and laterally transferred by STM manipulation, STM allows one to induce and detect additional states. On the one hand, an intermediate, flat configuration was observed (see Figure S7, Supporting Information). On the other hand, additional voltage pulses can yield additional products, presumably inducing multiple dehydrogenations or even decomposition of the $(BN)_3$ ring. An identification and classification of all potential products is beyond the scope of this work. However, we envision further studies aiming for the construction of distinct nanoscale *h*BN aggregates exclusively by STM manipulation of borazine, e.g., by promoting intermolecular bond formation, to be rewarding.

Finally, the structural analogy of the six-membered ring in borazine to the well-studied benzene molecule[51–54] allows for a comparison of these two systems. Benzene molecules adsorb in a flat geometry on (111) facets of coinage metal substrates, including Ag, at the hcp-hollow sites.[55] The effective surface area for intact benzene was estimated to about 50 Å^2,[11] which is close the value we deduced from the striped borazine phase (42 Å^2). The azimuthal orientation of benzene on Ag(111) is fixed such that a superimposed triangle with corners at every other C atom is aligned with the [1-10] and equivalent crystal directions,[53] analogous to the alignment of the B–B axes in the case of borazine on Ag(111). The adsorption position of benzene can be controlled by introducing functional groups with either electron donating or withdrawing effect,[53] a strategy that also might be applicable to functionalized borazines. The adsorption height of benzene on Ag(111) amounts to 3.04 Å.[55] The theoretical value derived in this study for borazine (3.26 Å) is slightly larger, but both findings are consistent with a physisorption character of benzene and borazine on Ag(111). Dehydrogenation of benzene via voltage pulses with an STM was achieved on Cu(100).[56,57] The benzene manipulation product was identified via inelastic electron tunneling spectroscopy and DFT simulation as C_6H_5 fragment and shows an increased apparent height and a symmetry reduction in STM imaging. These finding were rationalized by a transition from a flat benzene adsorption geometry to an upright standing configuration upon dehydrogenation, similar to the case of borazine dehydrogenation introduced in this work.

4. Conclusion

We provide for the first time a real space characterization of individual borazine molecules on a solid support and demonstrate the self-assembly of distinct, highly ordered borazine architectures on Ag(111). With increasing exposure, a chiral, porous honeycomb-like network and dense-packed, striped arrays are achieved. Borazine is shown to adsorb nondissociative with its ring aligned in parallel to the surface. The low temperatures (< ≈150 K) requested for adsorption, STS revealing the surface state, and the small calculated adsorption energies signal a weak interaction of pristine borazine with Ag(111). Nonetheless, distinct adsorption sites (fcc and hcp hollow) are determined by our combined STM and DFT approach. With the N atoms consistently residing near on-top sites of the Ag(111) lattice, these two adsorption sites result in two distinct azimuthal borazine orientations. Furthermore, controlled dehydrogenation of single borazine molecules by STM manipulation using voltage pulses is demonstrated. The resulting borazine fragment features an upright standing adsorption geometry, corroborated by DFT calculations. Our results elucidate the characteristics of pristine borazine adsorbed on Ag(111) and thus provide a reference system for many advanced BN-doped interfacial systems, including surfaces patterned by functionalized borazines or graphene-like systems incorporating $(BN)_3$ units. Additionally, the controlled dehydrogenation demonstrates a single molecule level access to the multi-facetted chemistry of this seemingly simple molecule, opening prospects for the controlled, sequential synthesis of nanoscale *h*BN aggregates by STM manipulation protocols.

5. Experimental Section

The experiments were performed in a custom- built UHV chamber with a base pressure <3 × 10^{-10} mbar. STM and STS data were acquired with a CreaTec Fischer L-TSTM operated at 7 K. Images are recorded in constant current mode with an electrochemically etched tungsten tip. The setpoint and applied sample bias voltage are given in the respective figure captions. Images of surface dislocations and atomically resolved Ag(111) were employed to obtain the [1-10] and equivalent crystal high symmetry directions and the lateral calibration. The Ag(111) single crystals (MaTeck, SPL) were prepared by repeated cycles of sputtering with Ar^+ ions at 1 keV and annealing to 450–470 °C. After dosing borazine (Purity 99%, Katchem) through a nozzle, the samples were precooled and then transferred to the LT-STM. The dose values (specified in L) base on the reading of the pressure gauge and thus the actual borazine dose at the Ag sample is higher.

Dispersion corrected DFT calculations were performed in the FHI-aims simulation package.[58–60] The exchange and correlation terms were

described using PBE functionals.[61] Spin polarized calculations were employed to account for the behavior after homolytic bond separation in dehydrogenated species. For the adsorption energy calculations, a $3 \times 3 \times 3$ unit cell was modeled, where the bottom layer was exempt for geometry optimization while the remaining atoms were allowed to relax until residual forces on each atom were $< 1.0 \times 10^{-3}$ eV Å^{-1}. Tersoff–Haman STM simulations were performed by summing all the states within an energy-window at the Fermi level of size determined by the experimental bias voltage.[62]

Supporting Information

Supporting Information is available from the Wiley Online Library or from the author.

Acknowledgements

The authors acknowledge fruitful discussions with Ari P. Seitsonen and acknowledge generous computing time at the Max-Planck Computing and Data Facility. This work is supported by the European Research Council (ERC) Consolidator Grant NanoSurfs (No. 615 233). M.G. acknowledges funding by the H2020-MSCA-IF-2014 program under GA no.658070 (2DNano). W.A. acknowledges funding by the Deutsche Forschungsgemeinschaft (DFG, German Research Foundation) via a Heisenberg professorship.

Conflict of Interest

The authors declare no conflict of interest.

Author Contributions

The manuscript was written through contributions of all authors. All authors have given approval to the final version of the manuscript.

Data Availability Statement

The data that support the findings of this study are available from the corresponding author upon reasonable request.

Keywords

adsorption, Ag(111), borazine, dehydrogenation, scanning tunneling microscopy, scanning tunneling spectroscopy, self-assembly

Received: September 14, 2023
Revised: November 19, 2023
Published online: December 10, 2023

[1] A. Stock, E. Pohland, *Ber. Dtsch. Chem. Ges.* **1926**, *59*, 2215.
[2] R. Báez-Grez, R. Pino-Rios, *RSC Adv.* **2022**, *12*, 7906.
[3] M. D. R. Merino-García, L. A. Soriano-Agueda, J. D. D. Guzmán-Hernández, D. Martínez-Otero, B. Landeros Rivera, F. Cortés-Guzmán, J. E. Barquera-Lozada, V. Jancik, *Inorg. Chem.* **2022**, *61*, 6785.
[4] D. Marchionni, S. Basak, A. N. Khodadadi, A. Marrocchi, L. Vaccaro, *Adv. Funct. Mater.* **2023**, *33*, 2303635.
[5] A. E. Naclerio, P. R. Kidambi, *Adv. Mater.* **2023**, *35*, 2207374.
[6] D. Golberg, Y. Bando, Y. Huang, T. Terao, M. Mitome, C. Tang, C. Zhi, *ACS Nano* **2010**, *4*, 2979.
[7] Wang, X., Wang, H., Shi, J., *J. Mater. Res.* **2018**, *53*, 11242.
[8] I. H. T. Sham, C.-C. Kwok, C.-M. Che, N. Zhu, *Chem. Commun.* **2005**, 3547.
[9] S. Kervyn, O. Fenwick, F. Di Stasio, Y. S. Shin, J. Wouters, G. Accorsi, S. Osella, D. Beljonne, F. Cacialli, D. Bonifazi, *Chem.-Eur. J.* **2013**, *19*, 7771.
[10] J.-W. He, D. W. Goodman, *Surf. Sci.* **1990**, *232*, 138.
[11] M. T. Paffett, R. J. Simonson, P. Papin, R. T. Paine, *Surf. Sci.* **1990**, *232*, 286.
[12] A. P. Farkas, P. Török, F. Solymosi, J. Kiss, Z. Kónya, *Appl. Surf. Sci.* **2015**, *354*, 367.
[13] G. Dong, E. B. Fourré, F. C. Tabak, J. W. M. Frenken, *Phys. Rev. Lett.* **2010**, *104*, 096102.
[14] F. Orlando, R. Larciprete, P. Lacovig, I. Boscarato, A. Baraldi, S. Lizzit, *J. Phys. Chem. C* **2012**, *116*, 157.
[15] R. J. Simonson, M. Trenary, *J. Electron. Spectrosc. Relat. Phenom.* **1990**, *54*, 717.
[16] R. J. Simonson, M. T. Paffett, M. E. Jones, B. E. Koel, *Surf. Sci.* **1991**, *254*, 29.
[17] L. Haug, J. P. Roth, M. Thaler, D. Steiner, A. Menzel, S. Tosoni, G. Pacchioni, E. Bertel, *Phys. Chem. Chem. Phys.* **2020**, *22*, 11704.
[18] W. Auwärter, *Surf. Sci. Rep.* **2019**, *74*, 1.
[19] R. Dong, T. Zhang, X. Feng, *Chem. Rev.* **2018**, *118*, 6189.
[20] A. J. Mannix, B. Kiraly, M. C. Hersam, N. P. Guisinger, *Nat. Rev. Chem.* **2017**, *1*, 0014.
[21] J. Sun, C. Lu, Y. Song, Q. Ji, X. Song, Q. Li, Y. Zhang, L. Zhang, J. Kong, Z. Liu, *Chem. Soc. Rev.* **2018**, *47*, 4242.
[22] K. Zhang, Y. Feng, F. Wang, Z. Yang, J. Wang, *J. Mater. Chem. C* **2017**, *5*, 11992.
[23] P. Bachmann, F. Düll, F. Späth, U. Bauer, H.-P. Steinrück, C. Papp, *J. Chem. Phys.* **2018**, *149*, 164709.
[24] J. Felter, M. Raths, M. Franke, C. Kumpf, *2D Mater.* **2019**, *6*, 045005.
[25] A. Ruckhofer, M. Sacchi, A. Payne, A. P. Jardine, W. E. Ernst, N. Avidor, A. Tamtögl, *Nanoscale Horiz.* **2022**, *7*, 1388.
[26] I. Neogi, A. M. Szpilman, *Synthesis* **2022**, *54*, 1877.
[27] C. A. Brown, A. W. Laubengayer, *J. Am. Chem. Soc.* **1955**, *77*, 3699.
[28] D. Bonifazi, F. Fasano, M. M. Lorenzo-Garcia, D. Marinelli, H. Oubaha, J. Tasseroul, *Chem. Commun.* **2015**, *51*, 15222.
[29] D. Marinelli, F. Fasano, B. Najjari, N. Demitri, D. Bonifazi, *J. Am. Chem. Soc.* **2017**, *139*, 5503.
[30] C. Chen, K. Guo, Y. Zhu, F. Wang, W. Zhang, H. Qi, *ACS Appl. Mater. Interfaces* **2019**, *11*, 33245.
[31] M. M. Lorenzo-García, D. Bonifazi, *Chimia* **2017**, *71*, 550.
[32] M. Schwarz, M. Garnica, F. Fasano, N. Demitri, D. Bonifazi, W. Auwärter, *Chem.-Eur. J.* **2018**, *24*, 9565.
[33] A. Belser, K. Greulich, P. Grüninger, H. F. Bettinger, H. Peisert, T. Chassé, *ACS Appl. Mater. Interfaces* **2020**, *12*, 19218.
[34] N. Kalashnyk, P. Ganesh Nagaswaran, S. Kervyn, M. Riello, B. Moreton, T. S. Jones, A. De Vita, D. Bonifazi, G. Costantini, *Chem. - Eur. J.* **2014**, *20*, 11856.
[35] C. Sánchez-Sánchez, S. Brüller, H. Sachdev, K. Müllen, M. Krieg, H. F. Bettinger, A. Nicolaï, V. Meunier, L. Talirz, R. Fasel, P. Ruffieux, *ACS Nano* **2015**, *9*, 9228.
[36] W. Xiao, X. Feng, P. Ruffieux, O. Gröning, K. Müllen, R. Fasel, *J. Am. Chem. Soc.* **2008**, *130*, 8910.
[37] T. Jasper-Tönnies, M. Gruber, S. Ulrich, R. Herges, R. Berndt, *Angew. Chem., Int. Ed.* **2020**, *59*, 7008.
[38] F. Müller, S. Hüfner, H. Sachdev, R. Laskowski, P. Blaha, K. Schwarz, *Phys. Rev. B* **2010**, *82*, 113406.
[39] L. Merz, K.-H. Ernst, *Surf. Sci.* **2010**, *604*, 1049.

[40] I. Piquero-Zulaica, J. Lobo-Checa, Z. M. A. El-Fattah, J. E. Ortega, F. Klappenberger, W. Auwärter, J. V. Barth, *Rev. Mod. Phys.* **2022**, *94*, 045008.
[41] K. Müller, M. Enache, M. Stöhr, *J. Phys.: Condens. Matter* **2016**, *28*, 153003.
[42] J. I. Urgel, D. Ecija, W. Auwärter, A. C. Papageorgiou, A. P. Seitsonen, S. Vijayaraghavan, S. Joshi, S. Fischer, J. Reichert, J. V. Barth, *J. Phys. Chem. C* **2014**, *118*, 12908.
[43] G. B. Grad, P. Blaha, K. Schwarz, W. Auwärter, T. Greber, *Phys. Rev. B* **2003**, *68*, 085404.
[44] R. Laskowski, P. Blaha, K. Schwarz, *Phys. Rev. B* **2008**, *78*, 045409.
[45] M. Bokdam, G. Brocks, M. I. Katsnelson, P. J. Kelly, *Phys. Rev. B* **2014**, *90*, 085415.
[46] K. Verma, K. S. Viswanathan, *Phys. Chem. Chem. Phys.* **2017**, *19*, 19067.
[47] D. P. Malenov, A. J. Aladic, S. D. Zaric, *Phys. Chem. Chem. Phys.* **2019**, *21*, 24554.
[48] Y. Ye, W. Sun, Y. Wang, X. Shao, X. Xu, F. Cheng, J. Li, K. Wu, *J. Phys. Chem. C* **2007**, *111*, 10138.
[49] J. Eichhorn, S. Schlögl, B. V. Lotsch, W. Schnick, W. M. Heckl, M. Lackinger, *CrystEngComm* **2011**, *13*, 5559.
[50] M. Garnica, M. Schwarz, J. Ducke, Y. He, F. Bischoff, J. V. Barth, W. Auwärter, D. Stradi, *Phys. Rev. B* **2016**, *94*, 155431.
[51] W. Liu, V. G. Ruiz, G.-X. Zhang, B. Santra, X. Ren, M. Scheffler, A. Tkatchenko, *New J Phys* **2013**, *15*, 053046.
[52] W. Gao, W. T. Zheng, Q. Jiang, *J. Chem. Phys.* **2008**, *129*, 164705.
[53] D. P. Miller, S. Simpson, N. Tyminska, E. Zurek, *J. Chem. Phys.* **2015**, *142*, 101924.
[54] J. A. Garrido Torres, B. Ramberger, H. A. Früchtl, R. Schaub, G. Kresse, *Phys. Rev. Mater.* **2017**, *1*, 060803.
[55] W. Liu, F. Maaß, M. Willenbockel, C. Bronner, M. Schulze, S. Soubatch, F. S. Tautz, P. Tegeder, A. Tkatchenko, *Phys. Rev. Lett.* **2015**, *115*, 036104.
[56] L. J. Lauhon, W. Ho, *J. Phys. Chem. A* **2000**, *104*, 2463.
[57] M.-L. Bocquet, H. Lesnard, N. Lorente, *Phys. Rev. Lett.* **2006**, *96*, 096101.
[58] V. Blum, R. Gehrke, F. Hanke, P. Havu, V. Havu, X. Ren, K. Reuter, M. Scheffler, *Comput. Phys. Commun.* **2009**, *180*, 2175.
[59] A. Tkatchenko, M. Scheffler, *Phys. Rev. Lett.* **2009**, *102*, 073005.
[60] V. G. Ruiz, W. Liu, E. Zojer, M. Scheffler, A. Tkatchenko, *Phys. Rev. Lett.* **2012**, *108*, 146103.
[61] J. P. Perdew, K. Burke, M. Ernzerhof, *Phys. Rev. Lett.* **1997**, *78*, 1396.
[62] J. Tersoff, D. R. Hamann, *Phys. Rev. B* **1985**, *31*, 805.